Iranian Journal of Oil & Gas Science and Technology, Vol. 13 (2024), No. 1, pp. 74–96
http://ijogst.put.ac.ir

An Experimental Study on the Kinetics of Natural Gas Hydrate Formation in Pure Water Using NF Unit Gas at the Bandar Imam Petrochemical Plant

Mohammad Reza Amini[1], Ali Borsalani[2*], Alireza Azimi[3], Mostafa Narimani[4], and Masoumeh Mirzaei[5]

[1] PhD Candidate, Department of Chemical Engineering, Islamic Azad University, Omidiyeh Branch, Omidiyeh, Iran

[2] Assistant Professor, Department of Chemical Engineering, Islamic Azad University, Omidiyeh Branch, Omidiyeh, Iran

[3] Associate Professor, Department of Chemical Engineering, Islamic Azad University, Mahshahr Branch, Mahshahr, Iran

[4] Assistant Professor, Department of Chemical Engineering, Islamic Azad University, Omidiyeh Branch, Omidiyeh, Iran

[5] Associate Professor, Department of Chemical Engineering, Islamic Azad University, Mahshahr Branch, Mahshahr, Iran

Highlights

- Experimental kinetics of natural gas hydrate formation using real NF gas
- Hydrate formation in pure water under controlled conditions
- Effects of temperature and pressure on hydrate formation kinetics
- Experimental determination of mass transfer and diffusion coefficients
- Results useful for hydrate prediction in gas processing systems

Received*: May 18, 2025*; revised*: September 05, 2025;* accepted*: September 15, 2025*

Abstract

Understanding the conditions of gas hydrate formation is essential for the design and operation of natural gas transmission pipelines. These compounds have been investigated from both thermodynamic and kinetic perspectives. Despite substantial advances in the thermodynamic characterization of hydrates, their formation kinetics remain insufficiently understood and require further investigation. Accordingly, to determine the equilibrium conditions of natural gas hydrate formation, six independent experiments were conducted using natural gas samples obtained from the NF unit of the Bandar Imam Petrochemical Complex. The experiments were performed in a fixed-volume reactor at temperatures of 278.3, 278.6, 284.8, 290.3, 279.3, and 280.6 K and corresponding pressures of 37.8, 19.3, 28.4, 52.2, 32.7, and 16.2 bar, respectively. The results indicated that the mass transfer coefficients were 0.343, 0.236, 0.200, 0.314, 0.297, and 0.166 m/s, whereas the molecular diffusion coefficients were 2.5968×10^{-9}, 6.2866×10^{-9}, 3.3931×10^{-9}, 1.49×10^{-9}, 4.28×10^{-9}, and 7.42×10^{-9} m²/s, respectively. These findings demonstrate that an increase in reactor temperature leads to a decrease in the mass transfer coefficient and an increase in the molecular diffusion coefficient. In contrast, an increase in pressure results in an increase in the mass transfer coefficient and a decrease in the molecular diffusion coefficient. These observed trends are consistent with established empirical correlations.

Keywords: Hydrate formation rate, Natural gas, Kinetics, Molecular diffusion coefficient, Mass transfer coefficient

[*] Corresponding author :
Email: ali.borsalani@iau.ac.ir

How to cite this article
Amini, M. R. et al., An Experimental Study on the Kinetics of Natural Gas Hydrate Formation in Pure Water Using NF Unit Gas at the Bandar Imam Petrochemical Plant, Iran J. Oil Gas Sci. Technol., Vol. 13, No. 1, p. 74–96, 2024. DOI: https://doi.org/10.22050/ijogst.2025.523830.1741

1. Introduction

Natural gas can facilitate the integration of renewable technologies and serve as a cleaner alternative to more carbon-intensive fossil fuels. However, energy generation from renewable sources such as wind and solar remains inherently intermittent and unstable (Gürsan and de Gooyert, 2021). One of the major operational challenges in gas transmission pipelines is the formation of gas hydrates, which can obstruct flow and cause severe equipment damage (Meng et al., 2025). Gas hydrates are ice-like crystalline solids formed when gas molecules are encapsulated within hydrogen-bonded cages of water molecules. These structures are stabilized under appropriate temperature and pressure conditions through hydrogen bonding among water molecules and van der Waals interactions between the guest gas molecules and the water lattice (Román-Pérez et al., 2010).

Hydrate formation occurs under specific conditions of low temperature and high pressure that stabilize the crystalline lattice. The process is exothermic and involves nucleation and growth stages, which are strongly influenced by parameters such as interfacial area, gas composition, and the presence of porous media or chemical additives. In contrast, hydrate dissociation is an endothermic process in which the crystalline structure decomposes into water and gas. This process can be induced by thermal stimulation, depressurization, or the injection of thermodynamic inhibitors and constitutes the fundamental mechanism for potential energy recovery from natural gas hydrate reservoirs.

Gas hydrates were first identified in 1810 by Sir Humphry Davy under laboratory conditions (Davy, 1810). More than 100 gas species, including methane, ethane, propane, butane, carbon dioxide, and hydrogen sulfide, are capable of forming hydrates in the presence of water under suitable thermodynamic conditions, many of which are present in natural gas mixtures (Aregbe, 2017). In 1934, Hammerschmidt established that hydrate formation was responsible for pipeline blockages, initiating systematic efforts to prevent and control this phenomenon (Hammerschmidt, 1934). In the late 1950s, Katz et al. (1959) conducted pioneering experimental investigations to determine the thermodynamic conditions for hydrate formation, thereby laying the foundation for understanding hydrate phase behavior in the oil and gas industry. Since that time, research on hydrate prevention and mitigation strategies has expanded considerably.

In 1966, Makogon proposed the natural occurrence of gas hydrates in geological environments characterized by favorable thermodynamic conditions (Makogon, 1966). The annual cost associated with hydrate prevention is estimated to be approximately one billion dollars, with chemical inhibition representing the most widely adopted mitigation strategy (Sloan and Koh, 2007). Odutola et al. (2021) demonstrated that polyvinyl caprolactam (PVCap) effectively suppresses methane hydrate formation. In a horizontal pipeline experiment, a PVCap concentration of 0.1% was identified as the optimal dosage for hydrate inhibition.

Several recent studies have evaluated the performance of various chemical inhibitors. Uzoigwe et al. (2022) experimentally investigated methanol, ethanol, and monoethylene glycol (MEG) for hydrate prevention and reported that methanol and ethanol were highly effective at a concentration of 2%, whereas MEG required a higher dosage to achieve comparable inhibition efficiency. Mehrabi et al. (2021) examined the effects of diethanolamine (DEA) and ethylene glycol (EG) on the phase equilibrium of methane hydrate and showed that these compounds shift equilibrium conditions, thereby acting as thermodynamic inhibitors. Pei et al. (2023) conducted experimental studies on different

chemical inhibitors in pipeline systems and demonstrated that certain inhibitors significantly prolonged the induction time and delayed hydrate formation. Kelland et al. (2021) reported that vinyl lactam-based polymers, such as polyvinylpyrrolidone (PVP) and PVCap, function as effective kinetic hydrate inhibitors (KHIs), and that their combined use with thermodynamic inhibitors such as MEG or methanol enhances overall inhibition performance. Wan et al. (2019) showed that natural polysaccharides can inhibit hydrate formation by increasing induction time and reducing the hydrate growth rate.

Despite their operational risks, gas hydrates have attracted substantial interest for applications in gas storage, water desalination, and gas separation technologies (Morozov et al., 2022). Because hydrates can store up to 180 times their own volume in the form of methane, they have been recognized as high-capacity systems for gas transport and storage, potentially offering safer, more economical, and environmentally sustainable alternatives to conventional methods (Hassanpour Youzband et al., 2024). Luo et al. (2022) reported increasing interest in hydrates as crystalline materials capable of compactly storing large volumes of gases, particularly carbon dioxide, which has stimulated research into their application in greenhouse gas capture and sequestration. Owing to their reversible formation and dissociation behavior, gas hydrates have also been investigated for gas sweetening, light hydrocarbon separation, seawater desalination, cold energy storage, and gas transportation (Viswanadhan et al., 2024; Liu et al., 2021; Chen et al., 2021; Koh et al., 2011).

Azimi et al. (2016) and related studies investigated hydrate formation for various gases and gas mixtures over a range of compositions (Manteghian et al., 2011; Bozorgian et al., 2020; Piramoon et al., 2019). Dhamu et al. (2024) demonstrated that the combination of L-tryptophan and 1,3-dioxane significantly promotes carbon dioxide hydrate formation in seawater, thereby enhancing gas sweetening processes. Song et al. (2024) showed that hydrate formation can be effectively employed for the separation of carbon dioxide and water from natural gas streams. Lee et al. (2024) examined the influence of epoxy cyclopentane concentration and reported that selecting an optimal promoter concentration significantly enhances hydrate-based gas storage capacity. Mu et al. (2024) found that tert-butyl methyl ether facilitates the formation of structure H hydrates, substantially improving methane storage capacity. Lv et al. (2022) demonstrated that ZIF-8 accelerates methane hydrate formation in pure water by reducing induction time.

Recent investigations have increasingly focused on hydrate formation kinetics, emphasizing parameters such as induction time, gas uptake rate, and mass transfer coefficients. Agarwal et al. (2019) presented a comprehensive review of hydrate kinetics and modeling approaches, Veluswamy et al. (2018) examined hydrate formation and dissociation in porous media, and Aman and Koh (2016) discussed the interfacial phenomena governing hydrate nucleation and growth. More recently, Wang et al. (2025) utilized a microfluidic platform to investigate methane hydrate formation and dissociation kinetics under multiphase conditions, providing detailed insights into pore-scale mechanisms and hydrate morphology. These studies provide an important benchmark for comparison with the present work.

Despite the extensive body of research on hydrate formation and inhibition, a significant gap persists in the experimental investigation of natural gas hydrate kinetics under authentic industrial gas compositions, particularly when untreated, multicomponent gas streams obtained directly from petrochemical facilities are used. Many prior studies have focused on model gases or pure methane, thereby neglecting the compositional complexity and operational variability inherent in real gas streams. Furthermore, kinetic investigations are frequently confined to theoretical simulations or highly simplified laboratory conditions.

To address these limitations, the present study experimentally evaluates the formation kinetics of natural gas hydrates in pure water using an actual gas sample collected from the NF unit of the Bandar Imam

Petrochemical Complex. The novelty of this work resides in the use of an industrially relevant gas mixture under controlled laboratory conditions to determine practical kinetic parameters, including mass transfer coefficients and molecular diffusivities, which can inform future hydrate modeling and mitigation strategies.

2. Experimental

2.1. Materials

The NF unit at the Bandar Imam Petrochemical Complex, located within the Mahshahr Special Economic Zone, is responsible for the reception and separation of natural gas liquids into lighter fractions, including ethane, propane, and butane. The unit primarily receives its feedstock from the South Oil-Rich Fields and the Bidboland-2 Gas Refinery. To investigate the kinetics of natural gas hydrate formation, the feed gas entering this unit was selected as the experimental sample. A gas sample with an initial pressure of 960 psi was directly collected from the pipeline, and its detailed composition is presented in Table 1.

The distilled water used in all experiments was supplied by Fajr Petrochemical Company. The unit conversion table applied throughout this study is provided in Table 2.

Table 1

Specifications of the natural gas mixture fed into the NF unit of the Bandar Imam Petrochemical Complex

Component	Mol.%
C_1 (mol%)	80.96
C_2 (mol%)	10.42
C_3 (mol%)	4.37
IC_4 (mol%)	0.28
NC_4 (mol%)	0.45
IC_5 (mol%)	0.1
NC_5 (mol%)	0.08
N_2 (mol%)	3.32
CO_2 (ppm)	1.17
C_6+ (mol%)	0.02

Table 2

Unit conversion table used in this study

Original Unit	SI Unit
1 cP × 1.0^{-3}	1 Pa·s
1 cSt × 1.0^{-6}	1 m²/s
1 psi × 6.8947573	1 Pa
1 Darcy × 9.86923×10^{-13}	1 m²

2.2. Hydrate formation apparatus

The experiments were conducted using a cylindrical, jacketed reactor fabricated from stainless steel SS-316, with an internal volume of 295 cm³ and a maximum allowable working pressure of 120 bar. To

enhance mixing efficiency and promote effective heat transfer between the reactor contents and the coolant, a rocking-type agitator capable of oscillatory motion was employed.

The reactor chamber was equipped with two high-pressure needle valves rated up to 6000 psi, allowing for gas and water injection as well as system discharge. The outer jacket was fitted with inlet and outlet ports to enable the circulation of a methanol-based coolant. Because hydrate formation is an exothermic process, an efficient cooling system was required to prevent premature hydrate dissociation. Therefore, all refrigerant lines and fittings were thermally insulated, and reactor temperature was controlled using a circulating chiller connected to the jacket.

Reactor pressure was monitored using a pressure transmitter with a measurement range of 0–100 bar and a precision of 0.01 MPa, which was connected to a digital display unit. Temperature measurements for both the reactor and the coolant loop were obtained using two temperature transmitters with an accuracy of ±0.1 K. Pressure and temperature data were continuously recorded at intervals ranging from one second to several minutes using Graph View software and subsequently transferred to a computer for further analysis. A schematic diagram of the experimental setup is presented in Figure 1.

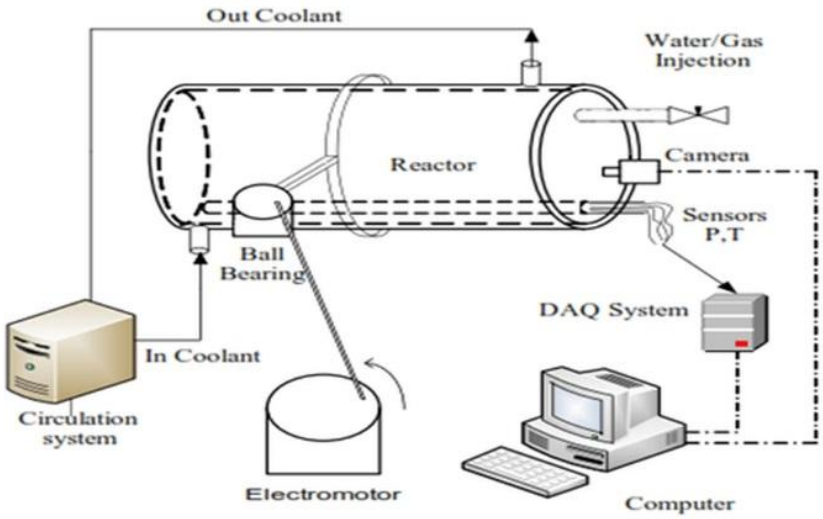

Figure 1

Schematic diagram of the laboratory system used to investigate gas hydrate formation

2.3. Experimental procedures

In this study, the Isochoric method was employed to determine hydrate formation equilibrium points (Sloan, 2008; Kvamme et al., 2009). Prior to the experiments, the reactor was cleaned with distilled water and subsequently dried using a vacuum pump. Then, 100 mL of water was introduced into the reactor at ambient temperature. A heat exchanger and circulator were used to control the temperature. Initially, the temperature of the heat exchanger was set, and methanol was circulated along the outer wall of the reactor. Three temperature sensors, each with an accuracy of 0.1 Kelvin, were installed inside the reactor. A pressure sensor with an accuracy of 0.1 bar was used to measure system pressure.

The procedure for obtaining the equilibrium point using the Isochoric method is illustrated in Figure 2. In this method, temperature and pressure are varied while maintaining a constant reactor volume. Initially, distilled water and natural gas were injected into the cell at a temperature higher than the equilibrium temperature (point A). Subsequently, the solution temperature decreased gradually due to the constant reactor volume, resulting in a corresponding gradual decrease in system pressure.

As the system temperature decreases and reaches point B, the hydrate formation process initiates, and the system pressure decreases sharply. Once the pressure stabilizes and hydrate formation is complete (point C), the temperature is gradually increased to induce hydrate decomposition. In the temperature–pressure diagram, the point at which the absorption and desorption curves intersect during the slow temperature increase (point D) represents the "hydrate equilibrium point."

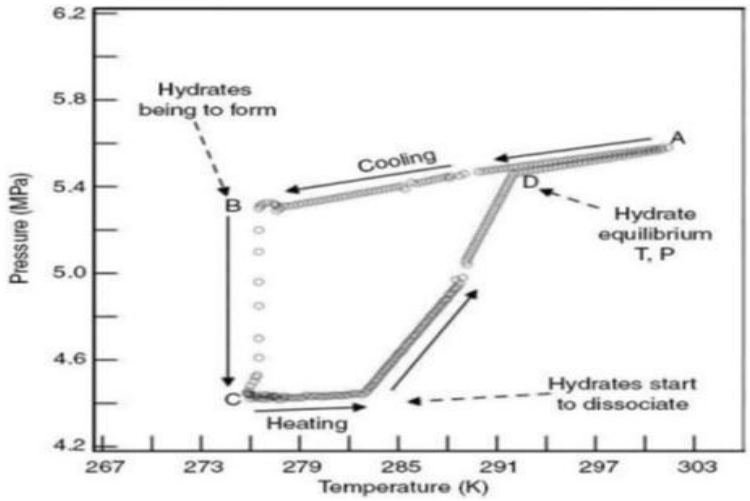

Figure 2

Determination of equilibrium points using the isochoric method (Sloan, 2008).

The Isochoric method typically involves two distinct stages: a cooling stage during which hydrate formation occurs and a subsequent heating stage that leads to hydrate dissociation. In the present study, only the hydrate formation stage was analyzed, as the primary objective was to determine key kinetic parameters, namely the molecular diffusion coefficient (DAB) and the mass transfer coefficient (Kc). Accordingly, Figures 3–5 have been revised to illustrate solely the hydrate formation stage.

3. Theoretical section

In this study, the number of moles of gas in the experimental system was calculated using real-time pressure and temperature data, together with the compressibility factor (Z). For natural gas under high-pressure conditions, the Peng–Robinson equation of state (PR-EOS) was employed to estimate Z. The detailed formulation of PR-EOS and its parameters are available in standard literature (Ahuja, 2008) and are omitted here for brevity.

To determine the compressibility factor (Z) of the gas, the cubic equation presented in Equation 1 must be solved, and the remaining parameters are calculated using Equation 2.

$$Z^3 - (1-B)Z^2 + (A - 3B^2 - 2B)Z - (AB - B^2 - B^3) = 0 \quad (1)$$

$$A = \frac{a\alpha P}{R^2T^2} \quad , \quad B = \frac{bP}{RT} \quad (2)$$

The compressibility factor (Z) for the gas mixture was estimated using the Peng–Robinson equation of state (PR-EOS) with standard mixing rules (Ahuja, 2008). The number of moles of gas present in the hydrate phase was calculated using an overall mass balance, as shown in Equation 3, where n_0 represents the initial number of moles of gas, n_v denotes the number of moles remaining in the gas phase after hydrate formation, and n_h corresponds to the number of moles incorporated into the hydrate phase.

$$n_0 = n_V + n_h \quad (3)$$

One of the most important kinetic parameters in the hydrate formation process is the mass transfer coefficient, which quantifies the rate of gas transfer. Based on previous studies, the empirical Equation 4 was employed to calculate this coefficient (Mohammadpour et al., 2019).

$$\frac{dn}{dt.A} = K_C.\frac{(P_i - P_{eq})}{RT} \rightarrow Q = K_C.\frac{(P_i - P_{eq})}{RT} \quad (4)$$

Where Q represents the molar flux of natural gas absorption, with units of mol/(cm²·s); P_i is the initial pressure in bar, P_{eq} is the equilibrium pressure in bar, R is the universal gas constant (83.14 bar·cm³/(mol·K)), and T is the reactor temperature in Kelvin. In this study, the value of Q was first calculated using the relation $Q = \frac{dn}{dt \cdot A}$, where dn is the change in the number of moles of gas over each time interval, and A, the cross-sectional area for mass transfer, was taken as 47.1 cm² for all experiments. Subsequently, the term $(P_i - P_{eq})/RT$ was computed at each time point using the experimental values of P_i and T. By plotting Q versus $(P_i - P_{eq})/RT$ for each experiment, the mass transfer coefficient K_C was determined from the slope of the fitted line.

The molecular diffusion coefficient D_{AB} is another critical parameter influencing mass transfer rates. Due to the limited availability of empirical correlations for this parameter, the following equation was employed in this study to calculate D_{AB} (Mohammadpour et al., 2018).

$$Q = 2C^* \sqrt{\frac{Dt}{\pi}} \quad (5)$$

In this equation, Q indicates the molar flux of natural gas absorption, expressed in mol/(cm²·s); C^* denotes the concentration of natural gas dissolved in water, in mol/cm³; D represents the diffusion coefficient of natural gas in water, in cm²/s; and t is time, in seconds. In this method, Q is plotted against $\sqrt{t}$, and the slope of the resulting line is determined. Using Equation 6, the diffusion coefficient of the gas mixture during hydrate formation can then be calculated.

$$D_{AB} = \frac{Slope^2 \times \pi}{4C^{*2}} \quad (6)$$

For this purpose, after determining the kinetics of natural gas consumption, the initial amount of gas introduced into the reactor was calculated. The consumed gas quantity, n_c, at each time point was then determined by subtracting the molar amount of gas remaining from the initial value. Subsequently, by plotting Q against $\sqrt{t}$, the experimental diffusion coefficient of natural gas during hydrate formation was calculated.

4. Results and discussion

4.1. Pressure variation of natural gas in pure water during hydrate formation in the NF unit of Bandar Imam Petrochemical Complex.

Figure 3 presents the pressure–time trajectories recorded during natural gas hydrate formation experiments (a–f), performed using deionized water and feed gas from the NF unit of Bandar Imam Petrochemical Complex. The plots are truncated at the point of hydrate formation completion to

emphasize the formation stage. In all experiments, a pronounced initial pressure decline is observed, corresponding to rapid gas uptake during the nucleation and early crystal growth phases. As hydrate formation progresses, the rate of pressure decrease diminishes, reflecting the gradual reduction in thermodynamic driving force and mass transfer efficiency. The profiles eventually reach a quasi-steady state, indicative of near-complete hydrate conversion and the establishment of equilibrium-like conditions within the system. This behavior is characteristic of Isochoric hydrate formation experiments and facilitates the extraction of key kinetic parameters, including induction time, apparent growth rate, and stabilization dynamics. The high reproducibility observed across replicate runs highlights the reliability and robustness of the adopted experimental protocol.

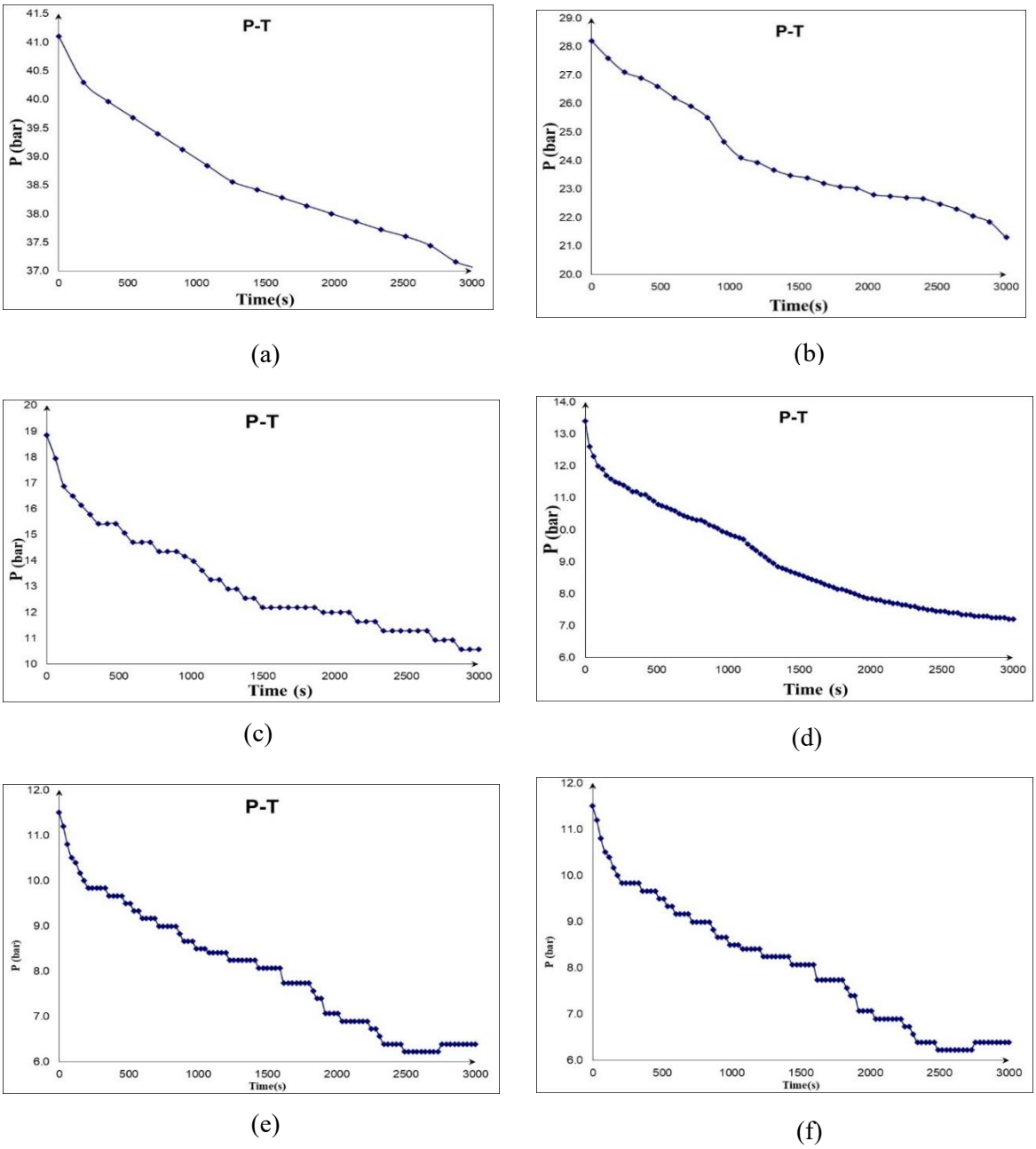

Figure 3

Pressure variations during natural gas hydrate formation in pure water in the NF unit of Bandar Imam Petrochemical Complex are shown for experiments (a) first, (b) second, (c) third, (d) fourth, (e) fifth, and (f) sixth. In the revised figure, only the pressure–time behavior up to the completion of hydrate formation is displayed. The

dissociation stage, which was employed solely to determine equilibrium points, has been omitted to avoid confusion and to focus exclusively on the hydrate formation process.

4.2. Variation in the number of moles of natural gas in pure water within the reactor of the NF unit, Bandar Imam Petrochemical Complex.

Figure 4 illustrates the temporal variation in the number of moles of natural gas within the reactor during hydrate formation. These values were determined by combining real-time measurements of pressure and temperature with the reactor volume, along with gas compressibility corrections using the Peng–Robinson equation of state. Data were recorded every 30 seconds using Graph View software, providing a detailed view of the gas consumption process. In all six experimental runs (a–f), a steady decline in the number of gas moles is observed, reflecting the progressive uptake of gas during hydrate formation. The steepest decrease occurs at the beginning of the process, corresponding to the nucleation and early crystal growth phases. As the experiments proceed, the slope of the curves becomes more gradual, indicating a reduction in the driving force for hydrate formation and increased limitations in mass transfer. By the end of the monitored period, the curves reach a plateau, consistent with the completion of hydrate formation under Isochoric conditions. Minor variations between runs can be attributed to differences in induction time, slight temperature gradients, or variations in nucleation initiation. Collectively, these results demonstrate that hydrate formation proceeds rapidly under kinetic control initially, but slows as thermodynamic and diffusional limitations become dominant, a trend that was reproducible across all experiments.

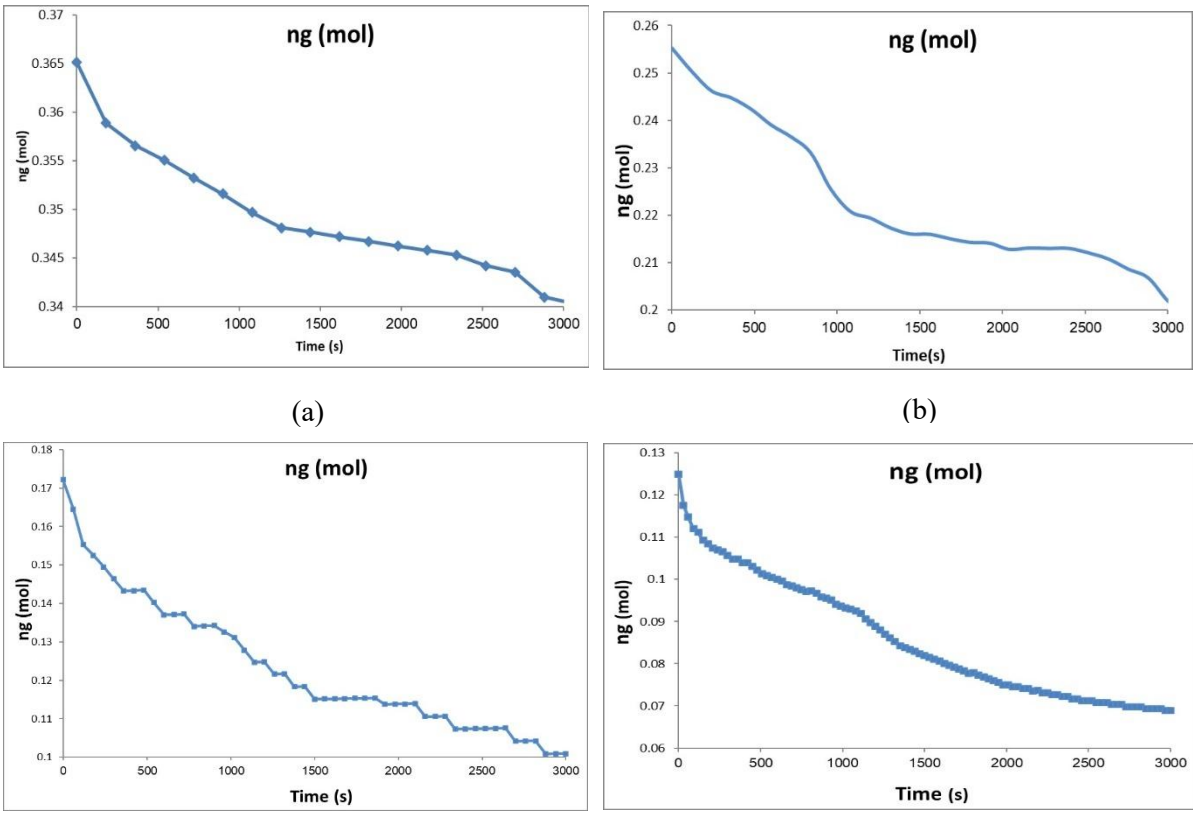

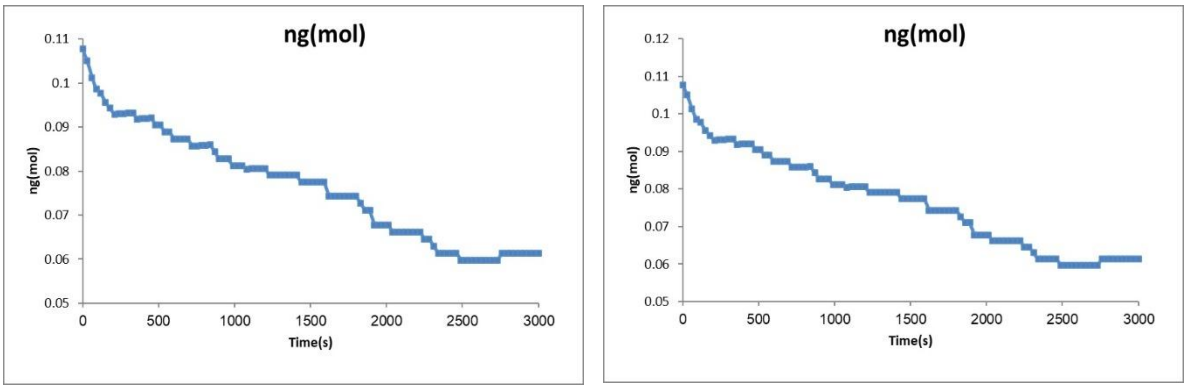

(e) (f)

Figure 4

Variations in the number of moles of natural gas hydrate formed in pure water in the NF unit of Bandar Imam Petrochemical Complex are shown for experiments (a) first, (b) second, (c) third, (d) fourth, (e) fifth, and (f) sixth. In the revised figure, only data up to the completion of hydrate formation are presented, while the dissociation stage has been excluded for clarity and to emphasize the formation process.

4.3. Kinetics of natural gas consumption in pure water during hydrate formation in the NF unit of Bandar Imam Petrochemical Complex

Figure 5 illustrates the temporal evolution of the cumulative number of moles of natural gas absorbed in the reactor during hydrate formation experiments (a–f). The absorbed gas was determined by comparing the initial gas inventory with real-time mole values, corrected for compressibility using the Peng–Robinson equation of state. Time is reported in seconds, and gas uptake is expressed in gmol. In all experimental runs, the curves exhibit a sharp initial increase in gas absorption, corresponding to rapid nucleation and crystal growth at the gas–liquid interface. As hydrate formation progresses, the slope of the curves decreases, reflecting the gradual reduction in the thermodynamic driving force and the increasing impact of mass transfer resistance. Toward the end of the monitored period, the curves plateau, indicating the completion of hydrate formation under Isochoric conditions. Minor variations among the six runs can be attributed to differences in induction time, subtle temperature gradients, or variations in mixing efficiency. Collectively, these observations highlight the two-stage nature of hydrate formation: a rapid, kinetically controlled initiation phase followed by a slower growth regime dominated by transport limitations.

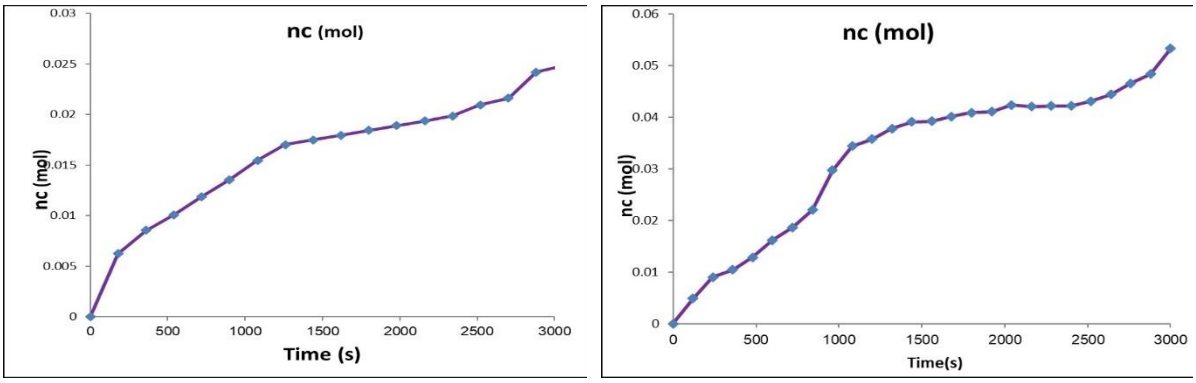

(a) (b)

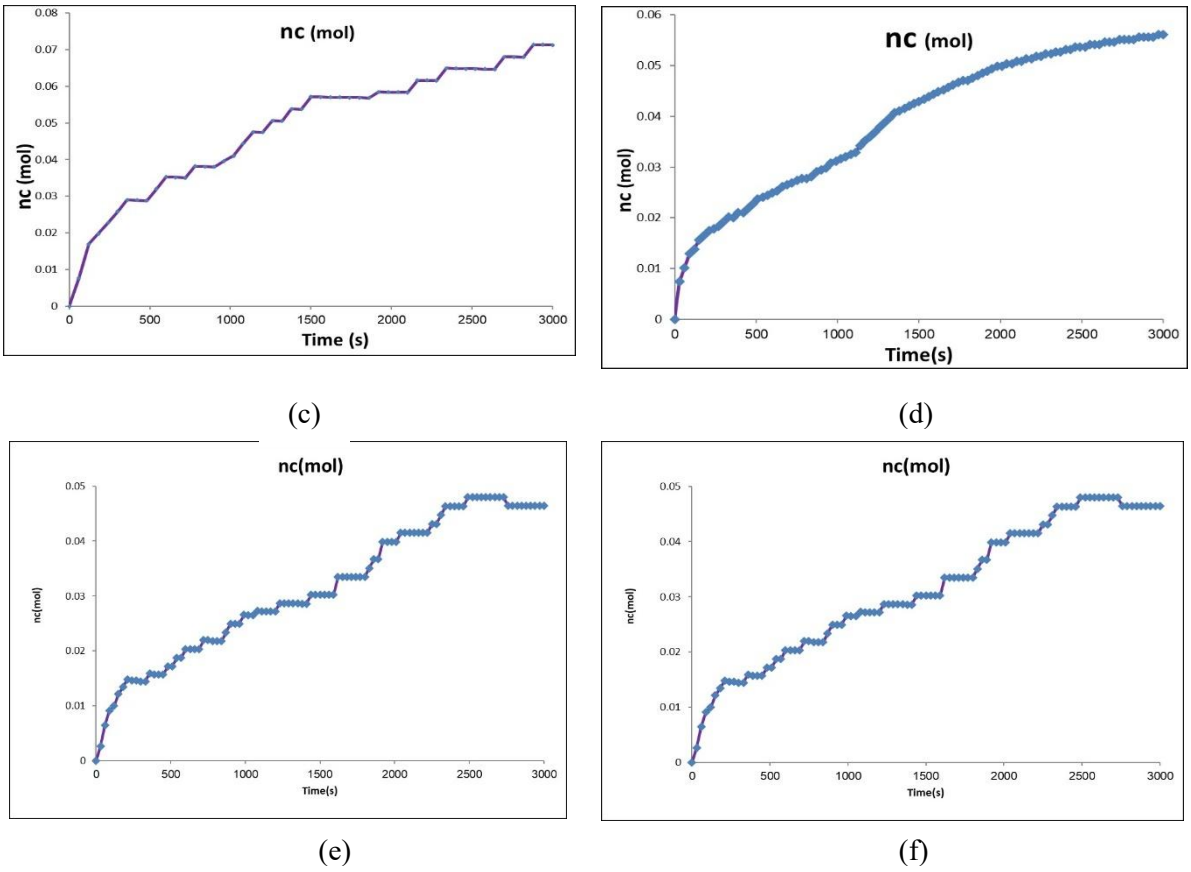

Figure 5

Variations in the number of moles of natural gas consumed in pure water in the NF unit of Bandar Imam Petrochemical Complex are shown for experiments (a) first, (b) second, (c) third, (d) fourth, (e) fifth, and (f) sixth. Consistent with the previous figures, only the hydrate formation stage is displayed, while the dissociation stage has been omitted to maintain clarity and emphasize the kinetics of hydrate formation.

4.4. Mass transfer coefficient of natural gas in pure water during hydrate formation in the NF unit of Bandar Imam Petrochemical Complex.

The experimental values of the mass transfer coefficient of natural gas in pure water for each of the six experiments conducted in the NF unit of Bandar Imam Petrochemical Complex were calculated using the algorithm described in Equation 4. The results are presented in the following table.

Table 3

Experimental values of the mass transfer coefficient for natural gas hydrate formation in pure water in the NF unit of Bandar Imam Petrochemical Complex.

Experiment number	Average temperature	Initial pressure	K_c (m/s)
1	278.3	37.8	0.343951411
2	278.6	19.3	0.236365493
3	284.8	28.4	0.200291318
4	290.3	52.2	0.31496
5	279.3	32.7	0.297317005
6	280.6	16.2	0.166293702

4.5. Molecular diffusion coefficient of natural gas in pure water during hydrate formation in the NF unit of Bandar Imam Petrochemical Complex

The experimental values of the molecular diffusion coefficient of natural gas in pure water for each of the six experiments conducted in the NF unit of Bandar Imam Petrochemical Complex were calculated using the algorithm outlined in Equations 5 and 6. The results are summarized in the following table.

Table 4

Experimental values of the molecular diffusion coefficient of natural gas in pure water in the NF unit of Bandar Imam Petrochemical Complex.

Experiment number	Average temperature	Initial pressure	D_{AB} (m²/s)
1	278.3	37.8	2.59678×10^{-9}
2	278.6	19.3	6.28661×10^{-9}
3	284.8	28.4	3.39308×10^{-9}
4	290.3	52.2	1.49×10^{-9}
5	279.3	32.7	4.28×10^{-9}
6	280.6	16.2	7.42×10^{-9}

Although the average temperatures in experiments 1 (278.3 K) and 2 (278.6 K) are very similar, the operating pressures in these two cases differ noticeably. This difference in pressure offers distinct insights into hydrate kinetics, as shown in Tables 3 and 4, where the impact of pressure variations on both the molecular diffusion coefficient (D_{AB}) and the mass transfer coefficient (K_c) is evident.

4.6. Statistical analysis of experimental results

The statistical analysis of the experimental data was performed using Design Expert software, version 13, and the results are presented in Tables 3 and 4 (Stat-Ease Inc., 2020). For this analysis, both the Response Surface Methodology (RSM) and the Historical Data method were employed. Two key variables influencing the kinetics of hydrate formation were introduced into the software: Parameter A represents the reactor pressure during hydrate formation, and Parameter B corresponds to the average reactor temperature. The effects of variations in these two parameters on the response factors—R_1: mass transfer coefficient (K_c) and R_2: molecular diffusion coefficient (D_{AB})—were experimentally examined and recorded. This section presents the statistical evaluation of how these input parameters influence the corresponding response variables.

4.7. Statistical analysis of parameters influencing the mass transfer coefficient

For each experiment conducted under different reactor temperature and pressure conditions, the mass transfer coefficient (K_c) was experimentally determined. These data were entered into the software as shown in Table 3. Following the statistical analysis, an empirical correlation for estimating the mass transfer coefficient (K_c) was derived and is presented below.

$$K_C = 0.24 + 0.13A - 0.078B + 0.021A.B \quad (7)$$

In Design Expert software, independent factors or inputs in an experiment (e.g., temperature, pressure, concentration) are by default labeled as '*A*' and '*B*,' while responses are labeled as '*R*.' The software often converts actual values (e.g., 50 °C, 100 °C) to a coded scale (e.g., –1, +1), and modeling is performed using these coded and normalized variables. Considering the interactions between the varying parameters, a statistical model was developed to estimate the mass transfer coefficient (K_c). The model demonstrated a high degree of reliability, with a coefficient of determination of $R^2 =$

0.9922. Figure 6 illustrates the variation of the mass transfer coefficient as a function of reactor pressure. As observed, an increase in reactor pressure leads to a significant rise in K_c. This effect is attributed to the enhanced solubility of natural gas in water and within the hydrate phase at higher pressures, which increases the frequency of gas–liquid interfacial molecular collisions. Consequently, both the rate of mass transfer and the corresponding coefficient in water are elevated.

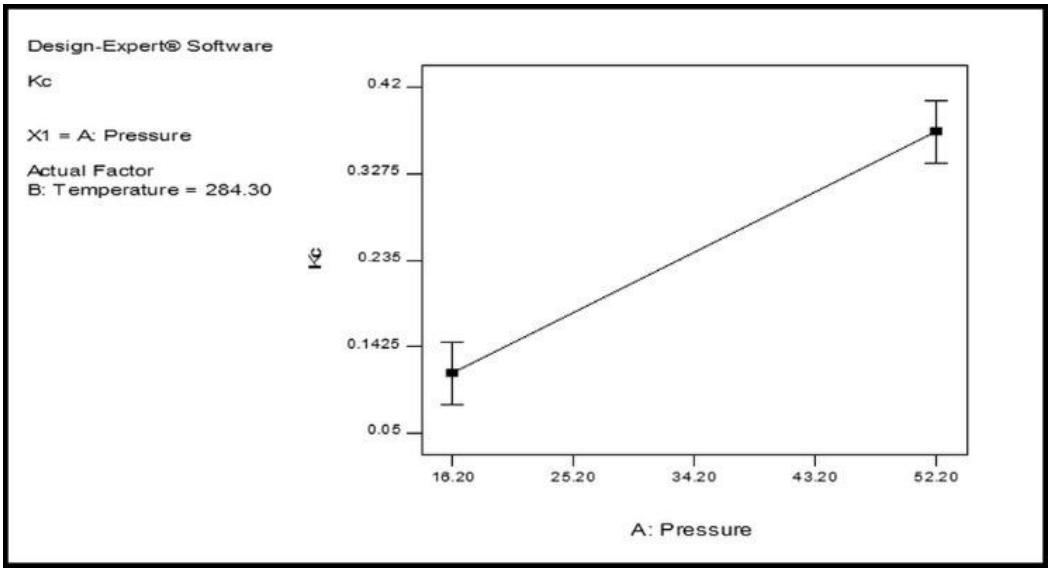

Figure 6

Variation of the mass transfer coefficient (K_c) with reactor pressure

Figure 7 illustrates the variation of the mass transfer coefficient (K_c) with reactor temperature. As shown, K_c decreases as the temperature increases. This inverse trend is attributed to the reduced solubility of natural gas in water and hydrate phases at elevated temperatures. Consequently, both the rate of mass transfer and the corresponding mass transfer coefficient in water decline.

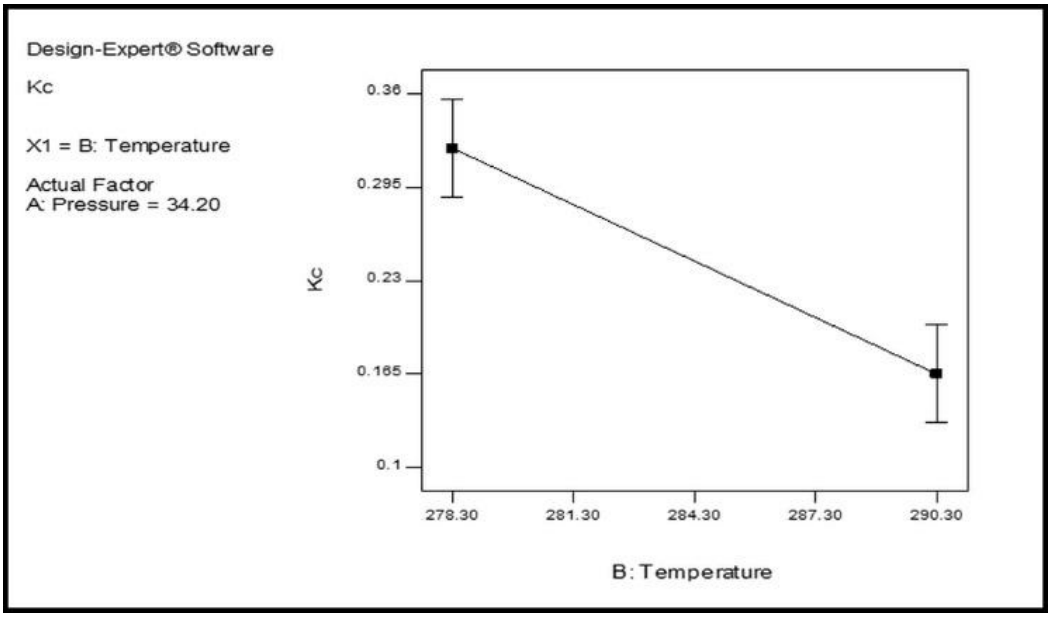

Figure 7

Variation of the mass transfer coefficient (K_c) with reactor temperature

In the preceding figures, the independent effects of each parameter influencing the mass transfer coefficient (K_c) were examined separately, without accounting for their mutual interactions. In the following section, the interaction effects between these parameters are evaluated. Figure 8 illustrates the combined influence of reactor temperature and pressure on the mass transfer coefficient (K_c).

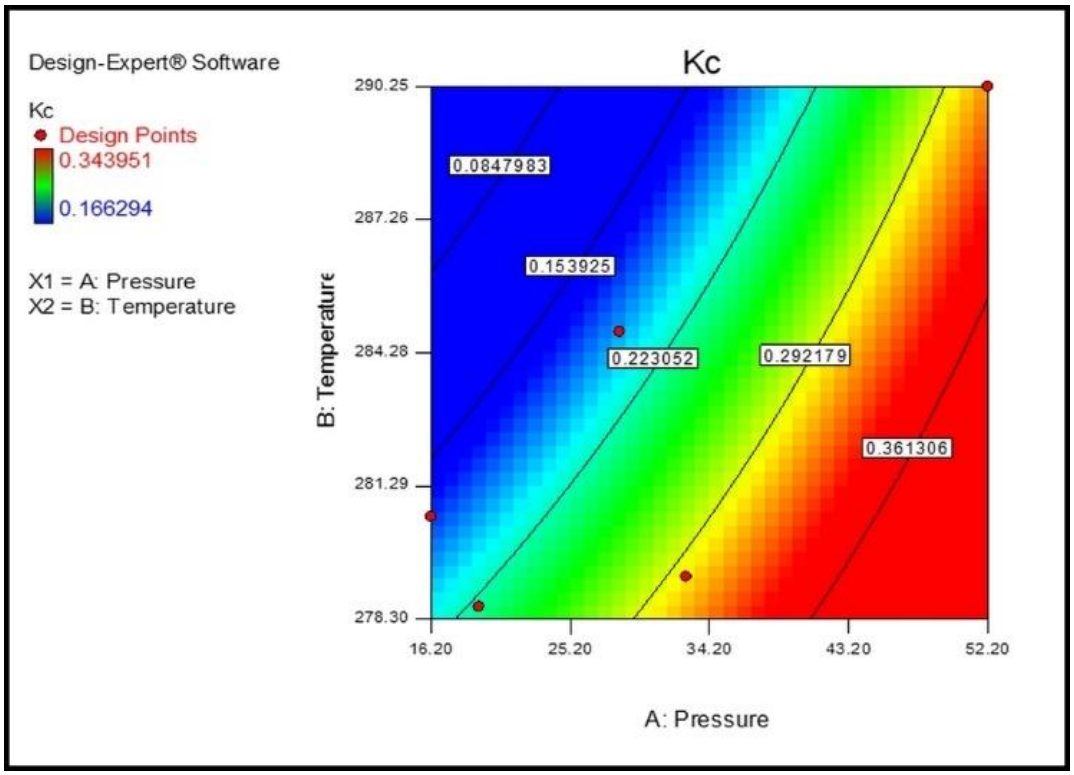

Figure 8

Effect of the combined interaction of reactor temperature and pressure on the mass transfer coefficient (K_c)

To assess the accuracy of the statistical model and its agreement with experimental data, the model-predicted values were compared with the values measured under laboratory conditions. As shown in Figure 9, the distribution of data points around the 45-degree line indicates a strong correlation between the model predictions and the experimental results, confirming the high reliability of the model developed using Design Expert software. The close agreement between experimental and predicted values, particularly in the mid-range regions, underscores the model's precision in simulating the behavior of the mass transfer coefficient. The coefficient of determination ($R^2 = 0.9922$) further validates the model's accuracy. Minor deviations are likely attributable to experimental uncertainties or operational fluctuations.

4.8. Statistical analysis of parameters influencing the molecular diffusion coefficient (D_{AB})

For each experiment conducted under varying temperature and pressure conditions, the molecular diffusion coefficient (D_{AB}) was experimentally determined. These values are presented in Table 4. Subsequently, following statistical analysis, Equation 8 was developed to predict the molecular diffusion coefficient (D_{AB}).

$$D_{AB} = 3.789 \times 10^{-9} - 2.979 \times 10^{-9}A + 1332 \times 10^{-9}B + 1.57 \times 10^{-10}A.B \quad (8)$$

Similar to the previous case, the coded variables *A* and *B* in the correlation represent reactor pressure and temperature, respectively, as defined by Design Expert software. Considering the interactions

between the varying parameters, the statistical model above was developed to estimate the molecular diffusion coefficient (D_{AB}) with a prediction accuracy of $R^2 = 0.9855$.

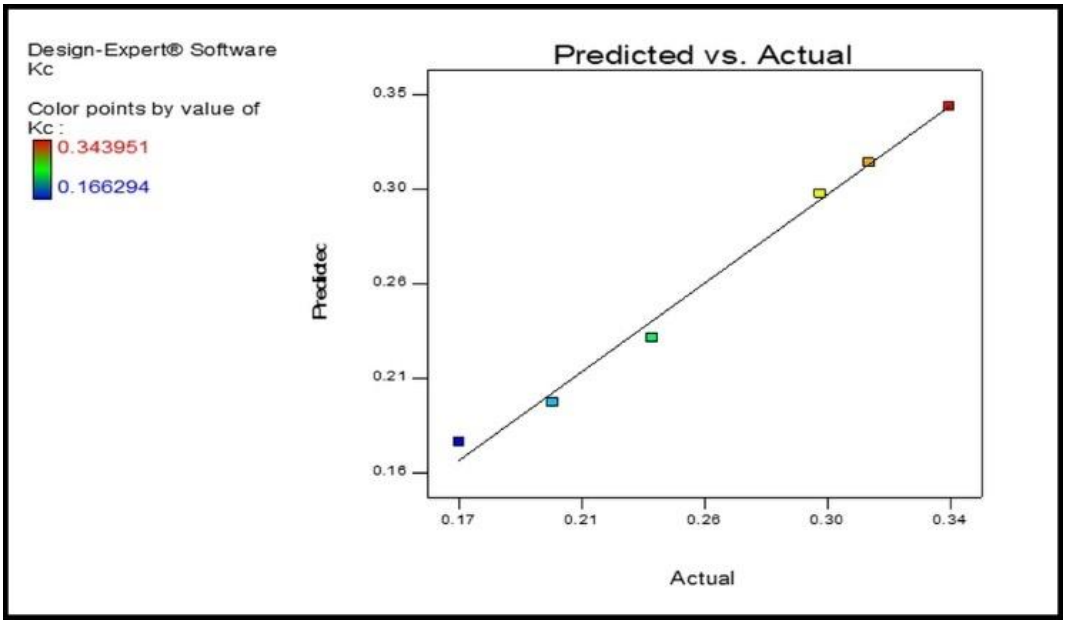

Figure 9

Comparison of experimental and predicted values of the mass transfer coefficient (K_c) using the statistical model developed in Design Expert software

Figure 10 illustrates the variation of D_{AB} with reactor pressure. As observed, the molecular diffusion coefficient decreases as reactor pressure increases. Theoretical studies have also shown that the molecular diffusion coefficient in gases declines with increasing pressure, primarily due to the corresponding increase in density and compressibility of the medium. This leads to a reduction in molecular transport velocity and, consequently, a decrease in the diffusion coefficient. In the present study, a nonlinear decrease in D_{AB} with increasing pressure was observed. Several empirical correlations have been proposed to describe this behavior, among which the Enskog and Chapman equations are notable. According to these models, the molecular diffusion coefficient is inversely related to pressure (Treybal, 1980).

$$D_{AB} = \frac{3}{16}\sqrt{\frac{2(RT)^3}{\pi}}\left(\frac{1}{M_A}+\frac{1}{M_B}\right).\frac{1}{\hat{N}p\delta_{AB}^2.\Omega_{DAB}} = 0.0018583\sqrt{T^3\left(\frac{1}{M_A}+\frac{1}{M_B}\right)}.\frac{1}{p\delta_{AB}^2.\Omega_{DAB}} \quad (9)$$

Figure 11 illustrates the variation of the molecular diffusion coefficient (D_{AB}) with reactor temperature. As shown, an increase in average temperature leads to an increase in D_{AB}. Previous studies have also theoretically demonstrated that rising temperature enhances the molecular diffusion coefficient. This phenomenon is attributed to the increased internal energy and molecular kinetic activity of gas molecules. In the present study, a nonlinear increase in D_{AB} was observed with increasing temperature. This behavior is consistent with the empirical Enskog and Chapman equations, which also predict a positive correlation between diffusion and temperature. Specifically, the molecular diffusion coefficient is proportional to temperature raised to the power of 1.5.

In the preceding figures, the individual effects of each parameter influencing the molecular diffusion coefficient (D_{AB}) were examined independently, without considering their interactions. Next, the combined interaction effects of these parameters are analyzed. Figure 12 illustrates the simultaneous interaction between average reactor temperature and pressure on the value of the molecular diffusion coefficient (D_{AB}).

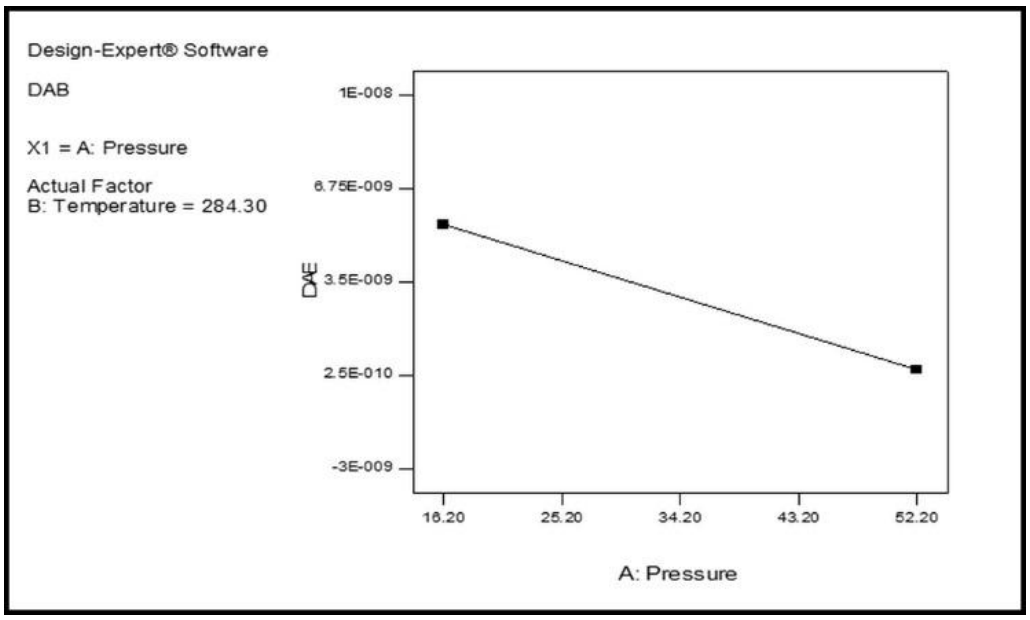

Figure 10

Variation of the intermolecular diffusion coefficient (D_{AB}) with reactor pressure

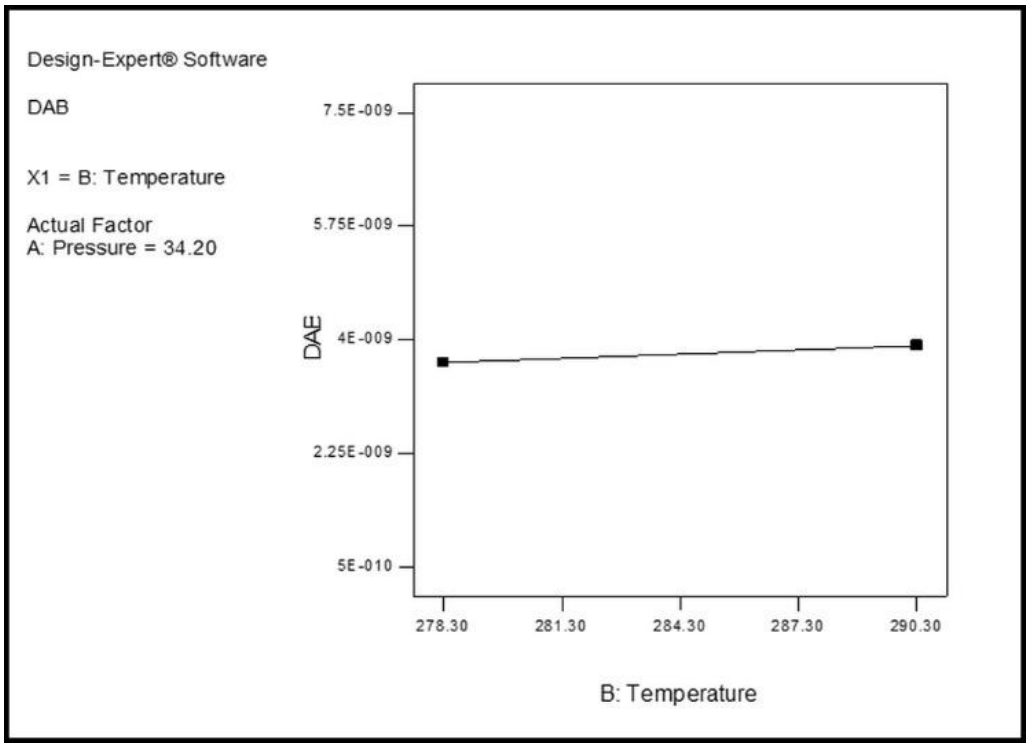

Figure 11

Variation of the intermolecular diffusion coefficient (D_{AB}) with reactor temperature

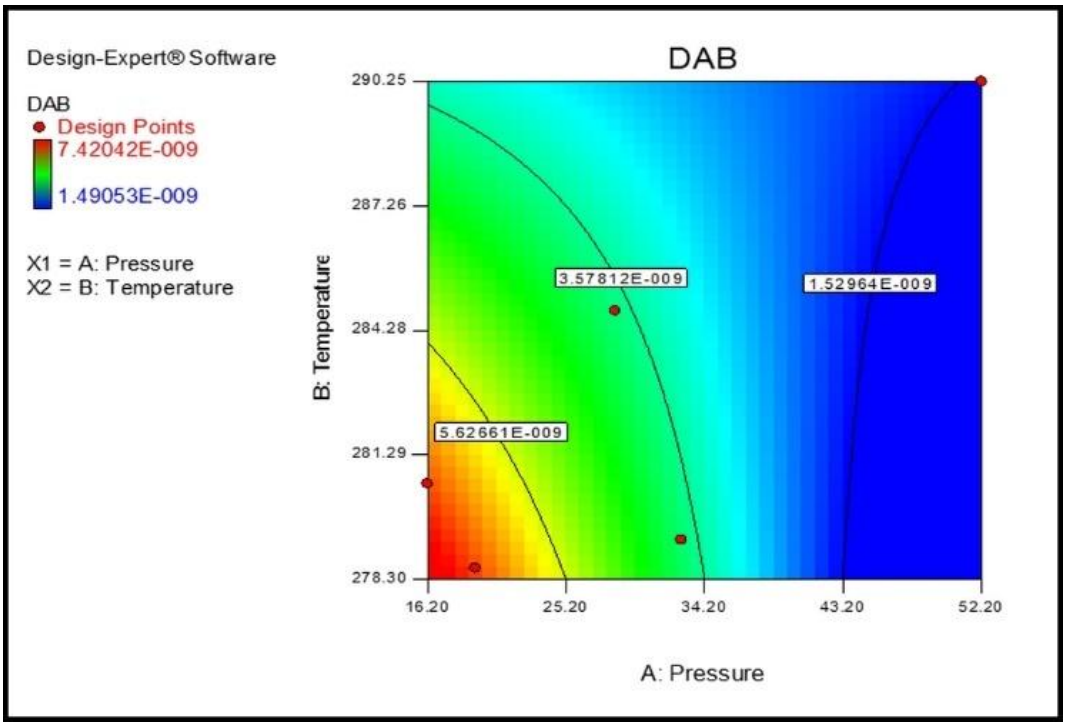

Figure 12

The effect of simultaneous interaction of temperature and pressure parameters in the reactor on the intermolecular diffusion coefficient (D_{AB})

4.9. Correlation analysis and interpretation of kinetic parameters

Using response surface methodology (RSM), two empirical models were developed to estimate key kinetic parameters, namely the mass transfer coefficient (K_c) and the molecular diffusion coefficient (D_{AB}), as functions of reactor pressure (A) and average reactor temperature (B). In these models, parameter A represents the operating pressure (in bar), while parameter B denotes the average reactor temperature (in Kelvin). The resulting correlations demonstrated excellent agreement with experimental observations, with coefficients of determination (R^2) of 0.9922 for K_c and 0.9855 for D_{AB}. These high R^2 values confirm the robustness and predictive accuracy of the statistical models for kinetic analysis and process simulation.

From a physical standpoint:

- Increasing pressure (A) enhances gas solubility in water and within hydrate structures, thereby improving the interfacial mass transfer rate and resulting in higher $K_c$values. However, higher pressure also leads to denser gas phases, which restrict molecular motion and thus reduce D_{AB}.
- Rising temperature (B) lowers gas solubility at the gas–liquid interface, leading to a decrease in K_c. Conversely, higher temperature increases molecular kinetic energy and mobility, thereby promoting diffusion and raising D_{AB}values.

These observed trends are consistent with classical theoretical models, specifically the mass transfer principles described by Treybal (1980) and the Chapman–Enskog (1970) theory of diffusion. According to the Chapman–Enskog formulation, the molecular diffusion coefficient is proportional to $T^{1.5}/P$, which aligns with the experimental results obtained in this study. Unlike many previous investigations that employed pure gases or binary mixtures, this study derives correlations from a real, multi-component natural gas stream under practical operational conditions. This significantly enhances the

industrial relevance and applicability of the developed models for field-scale hydrate modeling, simulation, and design.

The reliability of the developed correlations was assessed by comparing the obtained values of the mass transfer coefficient (K_c) and the molecular diffusion coefficient (D_{AB}) with literature data. As illustrated in Figures 13 and 14, the K_c values measured in this work (0.16–0.34 m/s) closely match the range reported by Azimi (2016) for hydrate-forming systems (0.18–0.32 m/s). Likewise, the diffusion coefficients calculated in this study (1.5×10^{-9}–7.4×10^{-9} m²/s) are consistent with the order of magnitude documented in the literature (Azimi, 2016). The observed variation of K_c and $D_{AB}$with temperature and pressure also follows theoretical expectations. Specifically, $K_c$increases with pressure but decreases with temperature, in agreement with the findings of Sloan (2008) and Englezos (1993). Similarly, D_{AB} shows a positive dependence on temperature and a negative dependence on pressure, consistent with the Chapman–Enskog relation ($D_{AB} \propto T^{3/2}/P$). These consistencies confirm the robustness of the developed correlations and demonstrate their alignment with both experimental and theoretical studies on hydrate kinetics.

Figure 13

Mass transfer coefficient (K_c) versus (a) temperature and (b) pressure, with comparison to Azimi (2016)

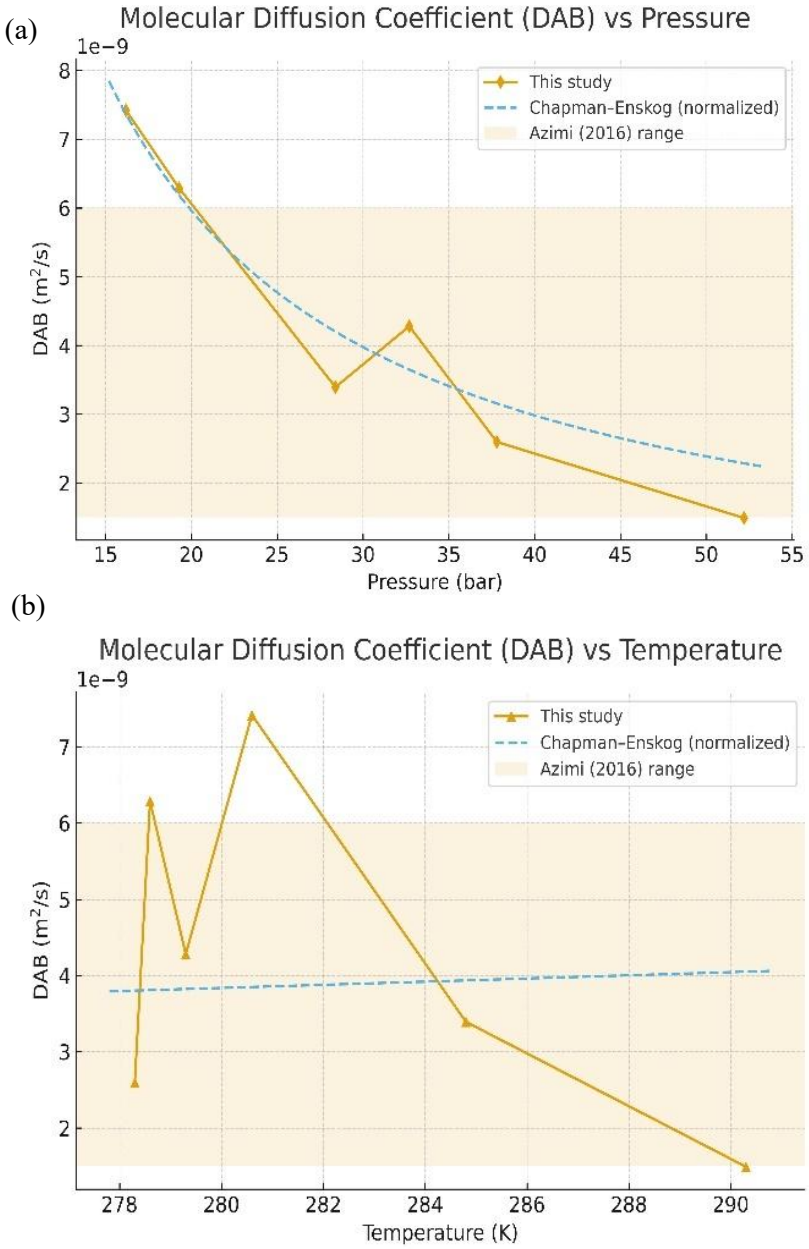

Figure 14

Molecular diffusion coefficient (D_{AB}) versus (a) temperature and (b) pressure, compared with the Chapman–Enskog relation and Azimi (2016)

5. Conclusions

In this study, a laboratory-scale experimental setup was utilized to examine the kinetic behavior of natural gas hydrate formation in pure water using a real, industrial gas mixture sourced from the NF unit of the Bandar Imam Petrochemical Complex. The main conclusions derived from both experimental observations and statistical modeling are summarized below:

- An increase in reactor temperature led to a reduction in the mass transfer coefficient (K_c), primarily due to the decreased solubility of natural gas in water at elevated temperatures. Conversely, an increase in reactor pressure significantly enhanced K_c by promoting gas solubility and increasing the frequency of gas–liquid molecular interactions.

- The molecular diffusion coefficient (D_{AB}) was found to increase with temperature due to enhanced molecular kinetic energy and to decrease with pressure, as higher density in the medium restricts molecular mobility. These trends are consistent with theoretical predictions from the Enskog and Chapman diffusion models.
- Statistical analysis revealed that pressure is the dominant factor influencing the mass transfer coefficient (K_c), whereas temperature has a more significant effect on the molecular diffusion coefficient (D_{AB}).

Industrial applicability

The experimentally derived kinetic parameters (K_c and D_{AB}), along with their corresponding empirical correlations, provide valuable inputs for the simulation, design, and optimization of hydrate prevention strategies in natural gas transportation systems, subsea pipelines, and storage facilities. These findings are particularly relevant for hydrate risk assessment and flow assurance modeling in real-world applications.

Suggestions for future work

To further enhance the understanding and applicability of hydrate formation kinetics, the following research directions are recommended:

- Explore hydrate formation behavior in saline or multi-component aqueous media.
- Evaluate the effects of chemical inhibitors and surfactants on K_c and D_{AB}.
- Integrate hydrodynamic variables such as flow velocity and turbulence into kinetic models.
- Apply the developed empirical models in CFD platforms or process simulators for scale-up studies and validation under field-representative conditions.

Acknowledgments

This article is derived from a doctoral dissertation entitled “Theoretical and Experimental Study of Natural Gas Hydrate Formation in the Presence of Surfactants: Tetra-n-butylammonium Chloride (TBAC) and Tetra-n-butylammonium Fluoride (TBAF),” conducted at the Department of Chemical Engineering, Omidiyeh Branch, Islamic Azad University, Omidiyeh, Iran.

Nomenclature

C_2H_6	Ethane
C_3H_8	Propane
CH_4	Methane
CO_2	Carbon dioxide
D_{AB}	Molecular diffusion coefficient
DEA	Di ethanolamine
gmol	Gram mole
H_2S	Hydrogen sulfide
K_c	Mass transfer coefficient
MEG	Mono ethylene glycol

NF Unit	Natural gas fractionation unit
PR-EOS	Peng–Robinson equation of state
PVC ap	Polyvinyl caprolactam
RSM	Response surface methodology
TBAC	Tetra-n-butyl ammonium chloride
TBAF	Tetra-n-butyl ammonium fluoride
Z	Compressibility factor
Greek symbols	
Δ	Difference
μ	Viscosity [cP]
$\emptyset$	Porosity, volume fraction
ρ	Density [kg/m³]
Subscripts	
eq	Equilibrium
i	Component i
s	Solvent
t	Time-dependent value
θ	Initial condition
Superscripts	
calc	Calculated value
exp	Experimental value
Sat	Saturated condition

References

Agarwal, A., Prasad, P. S. R., Sangwai, J. S., Ahuja, A., Ahuja, R., and Ahuja, R., A review on hydrate formation kinetics and modeling, Journal of Natural Gas Science and Engineering, Vol. 64, No. 1, p. 52–69, 2019.

Ahuja, P., Chemical Engineering Thermodynamics, PHI Learning Pvt. Ltd., 2008.

Aman, Z. M., and Koh, C. A., Interfacial phenomena in gas hydrate systems, Chemical Society Reviews, Vol. 45, No. 1, p. 1678–1690, 2016.

Aregbe, A. G., Gas hydrate—Properties, formation and benefits, Open Journal of Yangtze Oil and Gas, Vol. 2, No. 1, p. 27–44, 2017.

Azimi, A., and Mirzaei, M., Experimental Evaluation and Thermodynamic Modeling of Hydrate Selectivity in Separation of CO_2 and CH_4, Chemical Engineering Research and Design, Vol. 111, No. 1, p. 262–268, 2016.

Bozorgian, A., and Aboosadi, Z. A., Optimization of Determination of CO_2 Gas Hydrates Surface Tension in the Presence of Non-Ionic Surfactants and TBAC, Eurasian Chemical Communications, Vol. 2, No. 3, p. 420–426, 2020.

Chapman, S., and Cowling, T. G., The Mathematical Theory of Non-uniform Gases, 3rd ed., Cambridge University Press, 1970.

Chen, H., and Han, B., Hydrates for Cold Storage: Formation Characteristics, Stability, and Promoters, Applied Sciences, Vol. 11, No. 21, p. 10470, 2021.

Davy, H., On some of the combinations of oxymuriatic gas and oxygen, and on the chemical relations of these principles to inflammable bodies, Philosophical Transactions of the Royal Society of London, Vol. 100, No. 1, p. 231–257, 1810.

Dhamu, V., and Qureshi, M. F. A., Dual Promotional Effect of L-Tryptophan and 1,3-Dioxane on CO_2 Hydrate Kinetics in Seawater under Static/Unstatic Conditions for Carbon Capture and Storage Application, Energy & Fuels, Vol. 38, No. 13, p. 1-15, 2024.

Gürsan, C., and de Gooyert, V., The systemic impact of a transition fuel: Does natural gas help or hinder the energy transition? Renewable and Sustainable Energy Reviews, Vol. 138, No. 1, p. 110552, 2021.

Hammerschmidt, E. G., Formation of Gas Hydrates in Natural Gas Transmission Lines, Industrial and Engineering Chemistry, Vol. 26, No. 8, p. 851–855, 1934.

Hassanpour Youzband, A., and Joonaki, E., Gas storage via clathrate hydrates: Advances, challenges, and perspectives, Journal of Energy Storage, Vol. 65, No. 1, p. 107184, 2024.

Katz, D. L., Cornell, D., and Kobayashi, R., Handbook of Natural Gas Engineering, McGraw-Hill, New York, 1959.

Kelland, M. A., Zhang, Q., and Dirdal, E. G., Reliability and Performance of Vinyl Lactam-Based Kinetic Hydrate Inhibitor Polymers after Treatment under a Range of Conditions, Energy & Fuels, Vol. 35, No. 2, p. 1273–1280, 2021.

Lee, S., and Seo, D., Enhancing Hydrate-Based Natural Gas Storage Capacity via Optimal Concentrations of Epoxy cyclopentane, Chemical Engineering Journal, Vol. 502, No. 1, p. 157992, 2024.

Liu, G., and Zhu, L., New Technique Integrating Hydrate-Based Gas Separation and Chemical Absorption for the Sweetening of Natural Gas with High H_2S and CO_2 Contents, ACS Omega, Vol. 6, No. 39, p. 25640–25649, 2021.

Lv, X., and Bai, B., Study on the growth kinetics of methane hydrate in pure water system containing ZIF-8, RSC Advances, Vol. 12, No. 1, p. 21203–21212, 2022.

Makogon, Y. F., Features of natural gas fields exploitation in permafrost zone, Gazovaya Promyshlennost, Vol. 5, No. 1, p. 14–15, 1966.

Manteghian, M., and Azimi, A., Determination of CO_2 Hydrate Interfacial Tension in the Solution, Journal of Chemical Engineering of Japan, Vol. 44, No. 12, p. 936–942, 2011.

Mehrabi, K., Javanmardi, J., and Rasoolzadeh, A., Effects of diethanolamine and ethylene glycol + diethanolamine aqueous solutions on methane hydrate stability conditions: Experimental measurements and thermodynamic modeling, Journal of Molecular Liquids, Vol. 328, No. 1, p. 115428, 2021.

Meng, Y., Han, B., and Wang, J., Hydrate blockage in subsea oil/gas pipelines: Characterization, detection, and engineering solutions, Engineering, Vol. 46, No. 1, p. 363–382, 2025.

Mohammadpour, A., Mirzaei, M., and Azim, A., Dimensionless numbers for solubility and mass transfer rate of CO_2 absorption in MEA in presence of additives, Chemical Engineering Research and Design, Vol. 151, No. 1, p. 207–213, 2019.

Mohammadpour, A., Mirzaei, M., Azim, A., and Tababtabaei, S. M., The simultaneous effect of graphene oxide and sodium dodecyl sulphate nanoparticles on the kinetics of CO_2 absorption in amine solvent, Advances in Environmental Technology, Vol. 3, No. 1, p. 163–174, 2018.

Morozov, V., and Manakov, A., Gas Hydrates as High-Efficiency Storage System: Perspectives and Challenges, Energies, Vol. 15, No. 1, p. 8728, 2022.

Mu, L., and Zhou, Z., Experimental investigation on the methane storage by forming sH hydrate, Journal of Energy Storage, Vol. 77, No. 1, p. 109940, 2024.

Odutola, T. O., and Okomo, F., Performance of Poly Vinyl Caprolactam as Hydrate Inhibitor in a Prototype Horizontal Subsea Flowline, Petroleum Science and Engineering, Vol. 5, No. 2, p. 54–59, 2021.

Pei, J., Wang, Z., and Li, P., Experimental investigation on highly potent inhibitors of natural gas hydrate formation in a flow pipeline, Fuel, Vol. 347, No. 1, p. 127996, 2023.

Piramoon, H., and Moraveji, M., Experimental study of the formation of natural gas hydrates in the presence of NaCl and KCl, Petroleum Science and Technology, Vol. 37, No. 11, p. 1234–1242, 2019.

Román-Pérez, G., and Moaied, M., Stability, Adsorption, and Diffusion of CH_4, CO_2, and H_2 in Clathrate Hydrates, Physical Review Letters, Vol. 105, No. 1, p. 145901, 2010.

Selvaraj, Y., Song, Y., and Li, X., Natural Gas Hydrate, Far Beyond a Vast Resource of Natural Gas, The Innovation, Vol. 5, No. 1, p. 100074, 2024.

Sloan, E. D., and Koh, C. A., Clathrate Hydrates of Natural Gases, 3rd ed., CRC Press, p. 1–703, 2007.

Stat-Ease Inc., Design-Expert® Software, Version 13, Minneapolis, MN, USA, 2020.

Treybal, R. E., Mass Transfer Operations, 3rd ed., McGraw-Hill Book Company, 1980.

Uzoigwe, N. E., Comparing the Effectiveness of Methanol, Ethanol and Monoethylene Glycol at Preventing Hydrate Formation in a Hydrate Flow Loop, Uniport Journal of Engineering and Science Research, Vol. 6, No. 2, p. 12–17, 2022.

Veluswamy, H. P., Kumar, A., Seo, Y., Lee, J. D., and Linga, P., Gas hydrate formation and dissociation in porous media, Energy & Environmental Science, Vol. 11, No. 1, p. 979–993, 2018.

Viswanadhan, V., and Singh, A., Hydrate-based gas separation (HBGS) technology review: Status, challenges and way forward, Journal of Natural Gas Science and Engineering, Vol. 1, No. 1, p. 104710, 2024.

Wan, L., Zhang, N., and Liang, D. Q., Inhibition effects of polysaccharides for gas hydrate formation in porous media, Journal of Molecular Liquids, Vol. 293, No. 1, p. 111497, 2019.

Wang, Y., Yang, J., Wang, P., Zhu, J., and Chen, Y. J., Impact of multiphasic pore-scale interactions on gas hydrate formation and dissociation characteristics and kinetics: a microfluidic study, Lab Chip, Vol. 25, No. 1, p. 3741, 2025.